2008 International Symposium on Nonlinear Theory and its Applications
NOLTA'08, Budapest, Hungary, September 7-10, 2008

A computer-assisted proof of chaotic behaviour of the area preserving Hénon map

Balázs Bánhelyi,† Tibor Csendes,† and Barnabas M. Garay‡

†University of Szeged, Institute of Informatics
H-6701 Szeged, Hungary
‡Budapest University of Technology, Institute of Mathematics
H-1521 Budapest, Hungary
Email: banhelyi | csendes@inf.u-szeged.hu, garay@math.bme.hu

Abstract—The problem of finding transition graphs with complicated structure (complicated enough to imply the existence of horseshoe–type chaos in dynamical systems) is reformulated as a constraint satisfaction problem in optimization theory. In order to find a chaotic region, our method combines a global optimization procedure and an interval arithmetic based checking routine. Computational results on the area–preserving Hénon map are presented.

1. Chaos and transition graphs

1.1. The underlying abstract results

Starting from the landmark paper by Mischaikow and Mrozek [9] on the Lorenz equation, computer–assisted proofs for chaos have become an integral part of dynamical systems theory.

What the computer is actually used for is the rigorous checking of a finite number of inclusions of the form

$$\mathcal{T}_j(W_j) \subset U_j \ , \quad j = 1, 2, \ldots, M, \tag{1}$$

where the W_j's and U_j's are suitable subsets of the phase space and the $\mathcal{T}_j$'s are functions associated with the dynamics. The collection of inclusions (1) is structured by the concept of transition graphs and forms a sufficient condition for chaos, more precisely, for the embeddability of a certain type of symbolic dynamics into the mapping or differential equation under investigation. Unfortunately, the W_j's and U_j's (and—in the differential equation case—the $\mathcal{T}_j$'s) are not a priori given but have to be found somehow.

In two dimension, the definition of the transition graph is particularly simple.

Let $Q_1, Q_2, \ldots, Q_N$ be pairwise disjoint, closed, solid quadrangles in $\mathbb{R}^2$ with pairs of opposite edges termed horizontal and vertical. Continuing the vertical edges by parallel half–lines, two closed, solid, vertical stripes—an upper stripe and a lower stripe—are attached to each quadrangle. The upper stripe and the quadrangle share the upper horizontal edge whereas the lower stripe and the quadrangle share the lower horizontal edge of the quadrangle. Together with the attached stripes, each quadrangle separates $\mathbb{R}^2$ to a left and a right part. They are open, topological half-planes. For $i = 1, 2, \ldots, N$, the union of the two attached stripes is denoted by E_i. Left and right vertical edges of Q_i are denoted by e_i^λ and e_i^ρ, respectively. The corresponding left and right topological half–planes are components of the set $\mathbb{R}^2 \setminus (Q_i \cup E_i)$. They are denoted by $\mathcal{O}_i^\lambda$ and $\mathcal{O}_i^\rho$, respectively.

Definition 1 [9, 10, 6] *The transition graph $\mathcal{G} = \mathcal{G}(\varphi; Q_1, Q_2, \ldots, Q_N)$ of a continuous mapping $\varphi : \mathbb{R}^2 \to \mathbb{R}^2$ with respect to the collection of quadrangles $\{Q_1, Q_2, \ldots, Q_N\}$ is defined as the directed graph with vertex set $V(\mathcal{G}) = \{1, 2, \ldots, N\}$ and edge set $E(\mathcal{G})$ where $(i, j) \in E(\mathcal{G})$ if*

(i) $\varphi(Q_i) \subset \mathbb{R}^2 \setminus E_j$,

and one of the following two alternatives holds true:

(ii–a) *either* $\varphi(e_i^\lambda) \subset \mathcal{O}_j^\lambda$ and $\varphi(e_i^\rho) \subset \mathcal{O}_j^\rho$

(ii–b) *or* $\varphi(e_i^\lambda) \subset \mathcal{O}_j^\rho$ and $\varphi(e_i^\rho) \subset \mathcal{O}_j^\lambda$.

See Figure 1. The definition of the transition graph extends to collections of topological quadrangles, i.e., to collections of disjoint compact sets $\{\tilde{Q}_1, \tilde{Q}_2, \ldots, \tilde{Q}_N\}$, where $\tilde{Q}_i \subset \mathbb{R}^2$ is homeomorphic to a quadrangle Q_i (and the union of the two attached topological stripes $\tilde{E}_i$ is homeomorphic to E_i), $i = 1, 2, \ldots, N$. For the definition of transition graphs in higher dimension, see [7].

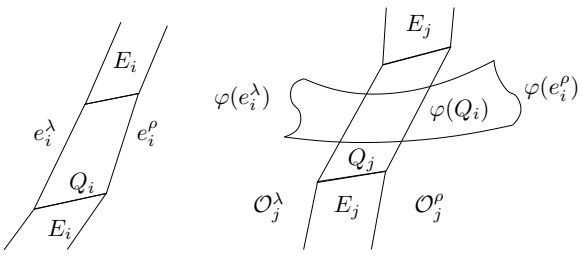

Figure 1: Conditions (i) and (ii–a)

Theorem 1 [9, 10, 6, 7] *Assume that the transition graph $\mathcal{G}(\varphi; Q_1, Q_2, \ldots, Q_N)$ contains two directed circles with nonempty intersection. Then φ admits horseshoe–type chaos on the set $X = \cup_{i=1}^{N} Q_i$. More precisely, a well–defined subshift dynamics on N symbols embeds in $\varphi|_X$, the restriction of φ to X.*

1.2. Examples

If, in particular, $N = 2$ and the transition graph $\mathcal{G}(\varphi; Q_1, Q_2)$ is the complete directed graph on two vertices, then Theorem 1 implies the existence of Σ_2–chaos: The full shift on two symbols embeds in $\varphi|_{Q_1 \cup Q_2}$. Examples include small perturbations of Smale's classical horseshoe mapping where, using the notation adapted in Figure 2, the set of inclusions (1) takes the form

$$\varphi(Q_1 \cup Q_2) \subset \mathbb{R}^2 \setminus (E_1 \cup E_2) \qquad (cf.\ (i)),$$

$$\varphi(e_1^\lambda) \subset \mathcal{O}_2^\rho \quad \text{and} \quad \varphi(e_1^\rho) \subset \mathcal{O}_1^\lambda \qquad (cf.\ (ii-a)),$$

$$\varphi(e_2^\lambda) \subset \mathcal{O}_1^\lambda \quad \text{and} \quad \varphi(e_2^\rho) \subset \mathcal{O}_2^\rho \qquad (cf.\ (ii-b))\,.$$

Note that $\mathcal{O}_2^\rho \subset \mathcal{O}_1^\rho$ and $\mathcal{O}_1^\lambda \subset \mathcal{O}_2^\lambda$.

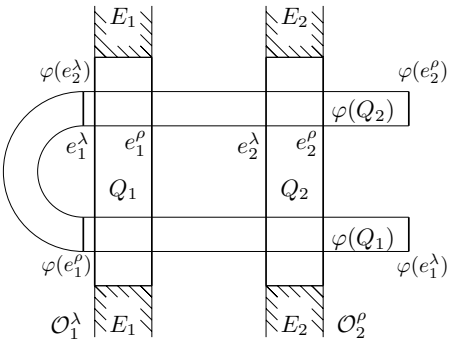

Figure 2: The classical Smale horseshoe

A topological copy of Figure 2 was found by Zgliczynski [10] in the phase portrait of the seventh iterate of the widely investigated *Hénon map*

$$\mathcal{H} : \mathbb{R}^2 \to \mathbb{R}^2\ ,\ (x, y) \to (1 - Ax^2 + y, Bx)$$

with the classical parameters $A = 1.4$ and $B = 0.3$.

See Figure 3 and observe the notational discrepancies between Figures 2 and 3. Rectangles Q_1 and Q_2 are replaced by parallelograms R and L, respectively. The vertical edges of L and R are denoted by a, b and c, d. The result of Zgliczynski [10] means that the full shift on two symbols embeds in $\mathcal{H}^7$ (more precisely, in $\mathcal{H}^7|_{L \cup R}$).

Theorem 2 [2] *The full shift on two symbols embeds in $\mathcal{H}^k$ if and only if $k = 2, 4$ or $k \geq 6$.*

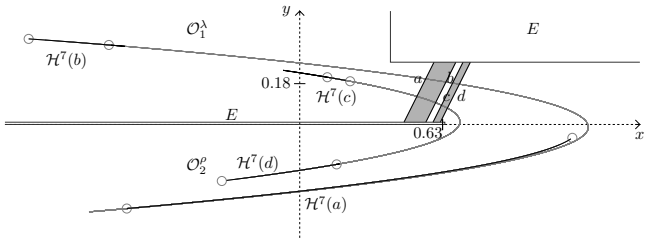

Figure 3: Sufficient condition for the horseshoe in $\mathcal{H}^7$

The proof of Theorem 2 is computer–assisted. Cases $k = 1, 3$ and $k = 5$ are excluded by analyzing periodic orbits. Cases $k = 2, 4$ and $k = 6, \ldots, 12$ are settled one by one via finding the respective pairs of quadrangles $\{Q_1(k), Q_2(k)\}$ for which $\mathcal{G}(\mathcal{H}^k; Q_1(k), Q_2(k))$ is the complete directed graph on two vertices. The remaining cases $k \geq 13$ are settled by an a posteriori theoretical argument.

1.3. The accompanying optimization problem

The proof of Theorem 2 differs strikingly from the usual computer–assisted proofs for chaos: There is no trial and error interaction between computer and computer scientist, and the tedious task of findig/adjusting the sets W_j, U_j in (1) by hand is left entirely to the computer. The search for the 'suitable' W_j's and U_j's can be interpreted [4, 1] as a constraint satisfaction problem in optimization theory and thus the application of global optimization algorithms for computer–assisted proofs of chaos becomes straightforward. Nevertheless, a reasonable choice of the search domain in the optimization procedure requires a 'good initial guess' for the W_j's and U_j's exploiting a priori numerical and theoretical results on the dynamics. This is the only reason why our method cannot be termed fully automatic.

Each relation $\mathcal{T}_j(W_j) \subset U_j$, $j = 1, 2, \ldots, M$ is analyzed separately. The j–th execution of Algorithm 1 discussed in detail in [4] may result in an interval $I_j = I_j(\lambda)$ such that $I_j \cap W_j \neq \emptyset$ but $T_j(I_j) \subset U_j$ does not hold true. This means that the j–th execution of Algorithm 1 ends at Step 10 – let $\mathcal{J} = \mathcal{J}(\lambda) = \{j_1, \ldots, j_\ell\} \subset \{1, 2, \ldots, M\}$ denote the set of such indices. Otherwise, for $j \notin \{j_1, \ldots, j_\ell\}$, the j–th execution of Algorithm 1 ends at Step 16.

ALGORITHM 1 *The Checking Routine*

Inputs:
- ε: the user set limit size — threshold — of subintervals,
- W: the argument set,
- U: the aimed set for which $\mathcal{T}(W) \subset U$ is to be checked.

1. Calculate the initial interval $I \supset W$

2. Push the initial interval into the stack
3. **while** (the stack is nonempty)
4. Pop an interval I out of the stack
5. Calculate the width of I
6. Determine the widest coordinate direction
7. Calculate the transformed interval $J = T(I)$
8. **if** $I \cap W \neq \emptyset$, and the condition $J \subset U$ does not hold, **then**
9. **if** the width of interval I is less than ε **then**
10. **print** that $\mathcal{T}(W) \subset U$ is hurt by I and **stop**
11. **else** bisect I along the widest side: $I = I_1 \cup I_2$
12. push the subintervals into the stack
13. **endif**
14. **endif**
15. **end while**
16. **print** that $\mathcal{T}(W) \subset U$ is proven and **stop**

Consider the optimization problem

$$\min_{\lambda \in \Lambda} g(\lambda)$$

where

$$g(\lambda) = p\left(\sum_{j \in \mathcal{J}(\lambda)} \max_{v \in T_j(I_j(\lambda))} \inf_{u \in U_j(\lambda)} |u - v|\right) \quad (2)$$

with $p(r) = r + 1$ if r is positive and $p(r) = 0$ otherwise. Here $I_j(\lambda)$ is the interval returned by the checking routine for $j \in \mathcal{J}(\lambda)$ (and the empty set for $j \notin \mathcal{J}(\lambda)$), $\Lambda \subset \mathbb{R}^m$ is the search set (the compact set of admissible parameter values), and $p : \mathbb{R} \to \mathbb{R}$ is the penalty function. Note that the j's summation term $\max_{v \in T_j(I_j(\lambda))} \inf_{u \in U_j(\lambda)} |u - v|$ of the argument of the penalty function in (2) is a nondifferentiable function of λ and stands for the Hausdorff semidistance of the transformed subinterval $T_j(I_j(\lambda))$ to the set $U_j(\lambda)$, a value proportional to the measure of how much condition $J \subset U$ (i.e., condition $T_j(I_j(\lambda)) \subset U_j(\lambda)$, $j \in \mathcal{J}(\lambda)$ in Step 6 of Algorithm 1) is violated.

The computation of this Hausdorff semidistance requires some geometrical considerations. It is an elementary task provided that $W_j, U_j \subset \mathbb{R}^2$ and that the boundary of each $U_j(\lambda)$ consists of a moderate number of finite or infinite straight line segments.

The penalty function p adds a fixed penalty term in case at least one of the constraints is not satisfied. Hence, if an optimization algorithm leads to a parameter vector λ_0 with $g(\lambda_0) = 0$, then – at the same time – the built-in checking routine provides a guaranteed reliability computational proof of the respective subset relations $\mathcal{T}_j(\lambda_0)(W_j(\lambda_0)) \subset U_j(\lambda_0)$, $j = 1, 2, \ldots, M$. Unfortunately, due to the high degree of nonlinearity of the problem, it is well possible that the output of the optimization algorithm is inconclusive, even if $\min_{\lambda \in \Lambda} g(\lambda) = 0$.

The emerging global optimization problem has been solved by a clustering stochastic optimization method which goes back to [3]. This technique is able to find all global optimizer points in search domains of moderate dimension and does not use the differentiability of the objective function. For a detailed discussion of this optimization model and of the relevant techniques of global optimization, see [4].

In all the applications we report on, a typical parameter is a coordinate of a vertex of a quadrangle. The search domains for the coordinates of the individual vertices are suggested by the position of the periodic points of the Hénon map [5] as well as by basic facts about homoclinic saddles.

2. Results on the area preserving Hénon map

The Jacobian determinant of the Hénon map is constant and—independently on the particular value of parameter A—equals to $-B$. It would be nice to have an analogue of Theorem 2 for $B = \pm 1$ and for a wide range of parameter A. Unfortunately, the computational task in the area–preserving case $B = \pm 1$ is much harder than in the area–contracting case $B = 0.3$.

So we set $A = 6.2$ and apply our optimization method for the third iterate of the Hénon map both in the orientation–preserving case $B = -1$ and the orientation–reversing case $B = 1$. For brevity, the *Hénon map with parameters* $A = 6.2$ *and* $B = -1$ is denoted by $\mathcal{H}_{OP}$. We look for quadrangles L and R for which the transition graph $\mathcal{G}(\mathcal{H}_{OP}^3; L, R)$ is the complete directed graph on two vertices. Suggested by the position of the eight fixed points of $\mathcal{H}_{OP}^3$ (marked by dots in Figure 4 – boldface dots refer to fixed points of $\mathcal{H}_{OP}$ itself), the search domains for the horizontal coordinates of the individual vertices of L and R are chosen for

$$\begin{aligned} V_{ul}^{L,x} &\in [0.30, 0.50], \quad & V_{ur}^{L,x} &\in [0.35, 0.55], \\ V_{ll}^{L,x} &\in [0.20, 0.40], \quad & V_{lr}^{L,x} &\in [0.25, 0.45], \\ V_{ul}^{R,x} &\in [0.35, 0.55], \quad & V_{ur}^{R,x} &\in [0.40, 0.60], \\ V_{ll}^{R,x} &\in [0.25, 0.45], \quad & V_{lr}^{R,x} &\in [0.40, 0.60], \end{aligned}$$

whereas the vertical coordinates are kept fixed. Those of the four upper vertices are taken for 0.50, those of the four lower verices are taken for 0.00. (The lower indices ul, ur, ll, lr stand for upper left, upper right, lower left, and lower right, respectively.)

The optimization algorithm ends up with the 'successful' collection

$$\begin{aligned} V_{ul}^{L,x} &= 0.35634938, \quad & V_{ur}^{L,x} &= 0.46734978, \\ V_{ll}^{L,x} &= 0.20136723, \quad & V_{lr}^{L,x} &= 0.38224280, \\ V_{ul}^{R,x} &= 0.54118627, \quad & V_{ur}^{R,x} &= 0.59341413, \\ V_{ll}^{R,x} &= 0.42762382, \quad & V_{lr}^{R,x} &= 0.54672081. \end{aligned}$$

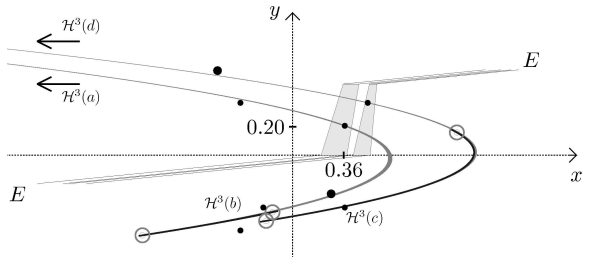

Figure 4: Optimization result for $\mathcal{H}^3_{OP}$ with $B = -1$.

Thus the full shift on two symbols embeds in $\mathcal{H}^3_{OP}|_{L\cup R}$. The result is illustrated in Figure 4.

Similarly, the full shift on two symbols embeds in the third iterate of the *Hénon map* $\mathcal{H}_{OR}$ *with parameters* $A = 6.2$ *and* $B = 1$. Now the horizontal coordinates of the respective quadrangles are

$$\begin{aligned} V^{L,x}_{ul} &= 0.37846661, \quad & V^{L,x}_{ur} &= 0.43276909, \\ V^{L,x}_{ll} &= 0.26337142, \quad & V^{L,x}_{lr} &= 0.34497950, \\ V^{R,x}_{ul} &= 0.44094381, \quad & V^{R,x}_{ur} &= 0.57439378, \\ V^{R,x}_{ll} &= 0.41452329, \quad & V^{R,x}_{lr} &= 0.49339729, \end{aligned}$$

whereas the vertical coordinates are as in the previous, orientation–preserving case. See Figure 5.

For $B = -1$ and $A > -0.866360$, Kirchgraber and Stoffer [8] prove the existence of a transversal homoclinic saddle in the Hénon map. By a famous result of Smale, it follows e.g. that the full shift on two symbols embeds in $\mathcal{H}^k_{OP}$, for k sufficiently large. Note that the proof in [8] is computer–assisted for $A \in (-0.866360, -0.265625)$.

Acknowledgments

The present work has been supported by the grants Aktion Österreich-Ungarn 70öu1, and OTKA T 048377 and T 046822. Balázs Bánhelyi was supported also by the Ferenc Deák Scholarship No. DFÖ 19/2007.

References

[1] B. Bánhelyi, T. Csendes, and B. M. Garay, "Optimization and the Miranda approach in detecting horseshoe-type chaos by computer", *Int. J. Bifurcation and Chaos*, vol. 17, pp. 735–747, 2007.

[2] B. Bánhelyi, T. Csendes, and B. M. Garay, "Σ_2 chaos for iterates of the classical Hénon mapping" (in preparation)

[3] T. Csendes, "Nonlinear parameter estimation by global optimization – efficiency and reliability", *Acta Cybernetica*, vol. 8, pp. 361–370, 1988.

[4] T. Csendes, B. M. Garay, and B. Bánhelyi, "A verified optimization technique to locate chaotic regions of a Hénon system", *J. Global Optimization*, vol. 35, pp. 145–160, 2006.

[5] Z. Galias, "Interval methods for rigorous investigations of periodic orbits", *Int. J. Bifurcation and Chaos*, vol. 11, pp. 2427–2450, 2001.

[6] Z. Galias, and P. Zgliczynski, "Abundance of homoclinic and heteroclinic connections and rigorous bounds for the topological entropy of the Hénon map", *Nonlinearity*, vol. 14, pp. 903–932, 2001.

[7] M. Gidea, and P. Zgliczynski, "Covering relations for multidimensional dynamical systems", *J. Differ. Eq.*, vol. 202, pp. 32–58, 2004.

[8] U. Kirchgraber, and D. Stoffer, "Transversal homoclinic points of the Hénon map", *Ann. Mat. Pura Appl.*, vol. 185, *suppl.* pp. 187–204, 2006.

[9] K. Mischaikow, and M. Mrozek , "Chaos in the Lorenz equations: a computer-assisted proof", *Bull. Amer. Math. Soc.*, vol. 32, pp. 66–72, 1995.

[10] P. Zgliczynski, "Computer assisted proof of the horseshoe dynamics in the Hénon map", *Random Comput. Dynam.*, vol. 5, pp. 1–17, 1997.

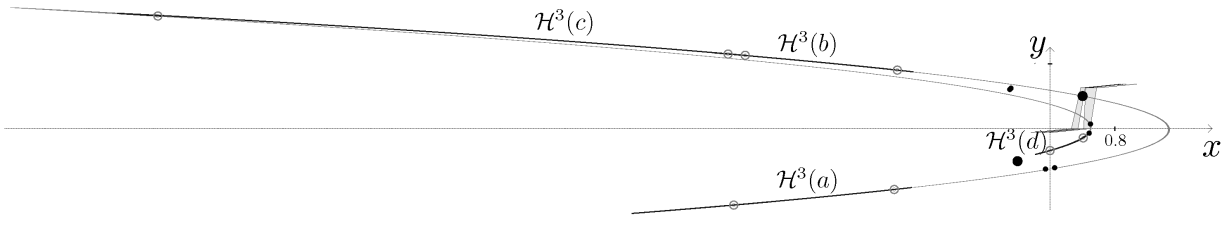

Figure 5: Optimization result for $\mathcal{H}^3_{OR}$ with $B = 1$.